Theoretical and experimental investigation of infrared properties of tapered silver/silver halide-coated hollow waveguides

Carlos M. Bledt,[1,2,*] Jeffrey E. Melzer,[1] and James A. Harrington[1]

[1]School of Engineering, Rutgers University, 607 Taylor Road, Piscataway, New Jersey 08854, USA

[2]School of Engineering, Brown University, 182 Hope Street, Providence, Rhode Island 02912, USA

*Corresponding author: carlos_bledt@brown.edu

Received 20 February 2013; accepted 3 April 2013;
posted 9 April 2013 (Doc. ID 185556); published 23 May 2013

Silver/silver halide-coated hollow-glass waveguides (HGWs) are capable of low-loss, broadband transmission at infrared wavelengths with the advantage of optical response tunability through alteration of a number of key design parameters. Generally, the design of circular HGWs has primarily involved optimization of the waveguide bore size and deposited film structure in order to obtain the desired optical response, with the waveguide bore size being held constant as a function of length. In this study, the effects of HGW structures consisting of linearly tapered inner diameters on the optical response at infrared wavelengths are theoretically and experimentally investigated. Theoretical analysis involving numerical ray optics methods accounting for the dynamic nature of bore size, and consequently light propagation, along the waveguide length is presented and compared to experimental results in order to gain a deeper understanding of these atypical HGW structures.

OCIS codes: (060.2390) Fiber optics, infrared; (080.2720) Mathematical methods (general).
http://dx.doi.org/10.1364/AO.52.003703

1. Introduction

Hollow-glass waveguides (HGWs) have been widely used in a variety of applications requiring the broadband, low-loss transmission of infrared radiation from $\lambda = 2.5$–12.0 μm where conventional optical fibers and other types of IR waveguides have little or limited functionality. In addition to their tunable optical response profile, HGWs enjoy several other attractive properties, including no end reflections, low output beam divergence, high coupling efficiencies, and mechanical rigidity [1]. HGWs consist of a fused silica capillary of fixed bore size (typically 200–1000 μm for practical applications) on whose inner surface a reflective silver film is deposited, essentially creating a high efficiency metallic cylindrical waveguide. To further enhance reflectivity of the inner HGW wall, a thin film, or stack of thin films, consisting of IR dielectric materials is deposited on the silver coated HGW [2]. Through modification of the deposited dielectric thin film thickness, the optical response of the waveguide may be modulated to optimize the structure for a desired wavelength(s).

The vast majority of research and development of HGWs has involved HGWs having length-independent constant bore size; thus the inner diameter dimensions remain unchanged along the entire waveguide length. Alternative HGW geometries that have been investigated in the past include square and rectangular polarization preserving waveguides and to a much lesser extent circular HGWs with length-dependent linearly tapered bore size [1,3–5]. This study focuses on the theoretical and implementation of tapered HGWs, particularly on their atypical beam propagating properties and their resulting IR response. Specifically, this analysis is carried out

1559-128X/13/163703-10$15.00/0

using a ray optics approach and comparing both theoretical and experimental results to those pertaining to constant bore HGWs. The theoretical and experimental results obtained in this study are furthermore contrasted to determine the feasibility and accuracy of the proposed ray optics approach in predicting tapered HGW waveguiding properties [4,6].

2. Theoretical Analysis

In developing an accurate and versatile theoretical model for predicting the atypical light propagating behavior of tapered HGWs, their dimensional differences relative to their constant bore counterparts must first be taken into consideration. In analyzing the effects of linearly length-varying bore size on the beam propagating properties, it is most convenient to take a ray optics approach that provides an excellent model due to the waveguide structural dimensions being much greater than the wavelength of light and that allows for natural consideration of geometrical differences in guide dimensionality [6].

In considering constant-bore HGWs, a propagating ray being coupled into the waveguide at a propagating angle of θ relative to the waveguide axis will propagate through the waveguide with a constant propagation angle of $|\theta|$, experiencing N reflections with the waveguide walls depending on both the total length, L, of the waveguide and the magnitude of the propagation angle. At each interaction with the waveguide walls, the light ray will experience reflection, R_i, that will depend on both the film structure and the complementary angle to the propagating angle (angle of incidence). Neglecting incoherent surface roughness related scattering, the reflectivity at each bounce will be constant, as ideally the propagating ray in a constant bore size HGW will remain the same. Through these considerations, in conjunction with trigonometric analysis of the system to derive the distance between successive reflections, the attenuation coefficient for a light ray propagating in a constant bore HGW can be accurately expressed by the expression given in Eq. (1) [1,2,6,7]:

$$\alpha(\theta,\lambda) = \frac{1 - R(\theta,\lambda)}{4a\ \cot(\theta)}, \tag{1}$$

where R is the propagation-dependent reflection coefficient per reflection (derived from the Fresnel coefficients) and a is the bore radius. This resulting attenuation derived through this ray-optics approach is in close concordance with that predicted for constant-bore HGWs derived through alternative wave optics approaches and has been widely considered to be highly accurate. Loss in constant-bore HGWs has been shown to vary as $1/a^3$, where a is the bore radius and as $1/r$ where r is the radius of curvature [1,2].

In the case of a linearly tapered HGW, where the slope of the ID is a function of waveguide length making an angle φ with respect to the waveguide longitudinal axis, Eq. (1) no longer holds. The inability to implement Eq. (1) for nonconstant bore HGWs is due to the resulting changing propagation angle along the waveguide length for any given initial launch angle, and as such the reflection coefficient at each bounce is no longer equal as it has a strong angular dependence. The dynamic nature of the propagation angle for any given ray has important implications, as any given ray vector reflecting off the waveguide walls will change as a function of both the taper gradient and the total number of times that it interacts with the waveguide surface (thus on the total waveguide length). In particular, whether the taper slope is negative or positive in the direction of propagation of the ray, its direction will change at each reflection, thus effectively changing its reflectance at each interaction with the waveguide walls. As a result of the dynamic nature of the propagation angle, the number of reflections from the waveguide surface will change, along with the reflectivity at each interaction. Figure 1 gives the representative ray propagation (and propagation angle) that remains unchanged in constant ID HGW structures (a and b) in contrast with the dynamic nature of directional ray propagation found in tapered HGWs (c and d). Such dynamic systems found in tapered HGWs do not lend themselves to a generalized and accurate analytical solution, such as Eq. (1) for the case of a constant-bore HGW, and are best treated via numerical ray optics analysis.

A. Ray Tracing Algorithm

The ray-tracing algorithm developed to analyze tapered bore HGW structures consisted of iterative computational techniques to track the change in propagation angle of a given ray propagating through the waveguide, thus determining the number of reflections with the waveguide walls as well as the angle of incidence at each reflection. To determine the number of reflections for a given waveguide structure, the algorithm made use of the initial propagation angle θ_i, the total waveguide length, L, and the initial and final ID sizes of the guide, $2a_i$ and $2a_f$, respectively. For the straight waveguides analyzed in this study, the waveguide boundaries relative to the waveguide axis were determined from

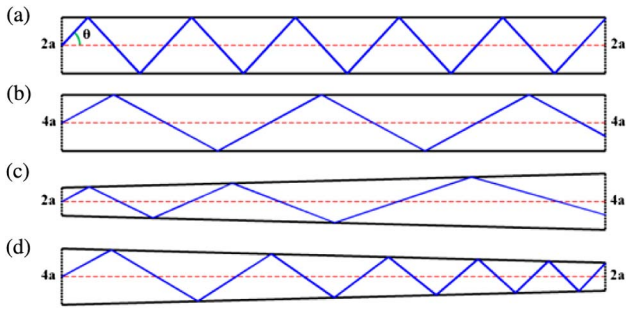

Fig. 1. Ray propagation in (a) smaller, (b) larger constant bore HGWs, (c) positive, and (d) negative linearly tapered bore HGWs.

the dimensions of the waveguide, yielding a linear equation describing the guide radius as a function of length. Given that the propagating rays are likewise linear and may thus be described by their y intercept and slope at any given point from the immediate initial position and angle of propagation, a system of equations may be constructed to solve for the intercepts of any propagating ray with the waveguide boundaries, signifying a point of reflection. From these vectors describing the waveguide boundaries and the propagating ray, the angle between the propagating ray and the waveguide wall may be obtained at any given point of intersection. This allows for determination of the angle of incidence and angle of reflection relative to the optic axis at that reflection point. By taking the coordinates of this point of intersection and both the direction and magnitude of the reflectance angle, the new initial points for determining the next interaction with the boundary imposed by the opposite waveguide surface may likewise be analyzed. This iterative procedure is repeated until the total length that the propagating ray has traveled in the direction parallel to the optic axis equals the total waveguide length. Equations (2) and 3 generalize the expressions for this iterative algorithm:

$$\begin{bmatrix} -\frac{a_f - a_i}{L} & 1 \\ -\tan^{-1}(\theta_{n-1}) & 1 \end{bmatrix} \begin{bmatrix} x_n \\ y_n \end{bmatrix} = \begin{bmatrix} a_i \\ y_{n-1} \end{bmatrix}, \tag{2}$$

$$\theta_n = -\frac{\theta_{n-1}}{|\theta_{n-1}|}(|\theta_{n-1}| - 2\varphi). \tag{3}$$

Implementing this methodology, the number of reflections of a propagating ray with a given initial propagation angle can be determined while simultaneously yielding numerical arrays of reflection coordinates (intersection points), angles of incidence at each of these critical points, and new propagation angles after each successive reflection. Through this analysis, the analytical expression for the new propagation angle after N reflections can be verified and the result is given by Eq. (4):

$$|\theta_N| = |\theta_i| - 2N\varphi, \tag{4}$$

where θ_i is the initial propagation angle and φ is the angle of the taper slope relative to the optic axis.

Calculation of the waveguide attenuation involves determining the reflectance at each successive reflection for the propagating ray. To achieve this, the incident angles at each reflection point as derived through the iterative ray tracing method described above is used as input to the ray transfer matrix method for the film structure in question, which in this case consists of a single AgI dielectric thin film ($n_d = 2.10$) and a reflective Ag film ($n_m = 13 - i56$) [8]. The total reflectance for a given propagating ray with dynamic propagation angle is then determined as the product of the individual reflectance values. From the total reflectance, the attenuation coefficient can be found.

B. Simulated Attenuation and Beam Propagation

Infrared propagation properties of linearly tapered Ag/AgI HGWs were theoretically analyzed using the aforementioned algorithm developed for this study. This study focused exclusively on the properties of tapered HGW structures with ID sizes varying from $2a = 650 - 300$ μm over a total waveguide length of 200 cm as these were the tapered waveguide dimensions used for the experimental part of this analysis. The HGW film structure pertaining to this study involved an Ag/AgI structure with dielectric AgI film thickness being selected for optimal performance between $\lambda = 9$–11 μm. In theoretical calculations, maximum coupling efficiency conditions were assumed with a Gaussian input beam having a FWHM diameter of 6.5 mm to yield the optimal coupling parameters given in Table 1 [1,6,7].

By utilizing the coupling parameters for the input Gaussian beam listed in the table above as input to the ray tracing algorithm developed for this study, theoretical losses for the 200 cm long, linearly tapered Ag/AgI HGWs optimized for maximum performance at $\lambda = 10.6$ μm were calculated. In the attenuation and beam propagation calculations, only meridional rays were considered, as skew ray propagation modeling is considerably more complex and their contribution to HGW transmission is negligible for any practical waveguide length due to their high losses. Table 2 gives the calculated attenuation for launch angles corresponding to HE_{11} mode coupling for the cases of increasing and decreasing bore size, as well as for 300 and 650 μm constant ID HGWs [1,2]. From the theoretical analysis and resulting calculations, several interesting observations can be made. As expected, the calculated attenuation for the tapered HGWs is between that of the constant 300 and 650 μm ID guides; yet it is not halfway between that of the two diameters, as this would correspond to a loss of 0.53 dB for a 200 cm long 475 μm ID HGW.

Table 1. Optimal Coupling Parameters

	$2a = 300$ μm	$2a = 650$ μm
Lens focal length	76.2 mm	127.0 mm
Corresponding $f/\#$	11.72	19.54
Depth of focus	3.71 mm	10.31 mm
Spot size ∅	158 μm	265 μm
Beam divergence	1.22°	0.73°

Table 2. Calculated HGW Attenuation

Input ID (μm)	300	650	300	650
Output OD (μm)	650	300	300	650
HGW length (cm)	200	200	200	200
Launch angle (°)	1.55	0.72	1.55	0.72
Output angle (°)	0.72	1.56	1.55	0.72
No. of reflections	83	84	180	39
Total attenuation (dB)	0.70	0.70	1.79	0.22

Additionally, it can be seen that the loss of the tapered HGWs is theoretically independent of input ID size, yet the output beam divergence angle is not. In fact, the beam divergence decreases when the guide is oriented with the smaller ID end as input and increases in the alternate case. As previously mentioned, the output divergence angle can be calculated if the number of reflections and launch angle are known through Eq. (4). In general, it can be noted that the number of reflections will increase as either the total waveguide length or taper gradient increases, resulting in increased attenuation and change in ray propagation angle.

In addition to considering the attenuation of linearly tapered HGWs through ray tracing analysis, the output beam propagation properties may be qualitatively and quantitatively examined. Calculating attenuation as a function of output angle via ray tracing techniques, the output spot size and beam divergence may be predicted. The simulations presented in Fig. 2 were derived for a 200 cm long straight waveguide along with output propagation angles ranging from $\theta_i = -5$ to 5° [1,7]. From Fig. 2, we see that the output spot size is indeed smaller when light propagates along the direction of increasing bore size than when it propagates in the direction of decreasing bore size. Furthermore, additional comparison shows that for the former case, beam narrowing occurs with increasing waveguide length while for the latter case, beam widening occurs with increasing waveguide length as predicted by Eq. (4). Additional output beam propagation analysis involved determination of the divergence angles in both cases by obtaining the full width at half-maximum of the projected beam profiles at distances of 10, 20, 30, 40, and 50 mm from the waveguide output using the information in Fig. 2. The resulting FWHM/projection distance dependence for both straight tapered HGW configurations is presented in Fig. 3. Using the methodology presented in Fig. 3, the theoretical divergence half-angles for 200 cm long straight, linearly tapered HGWs were determined to be 1.00° and 0.46° for light traveling in the direction of decreasing and increasing bore size, respectively.

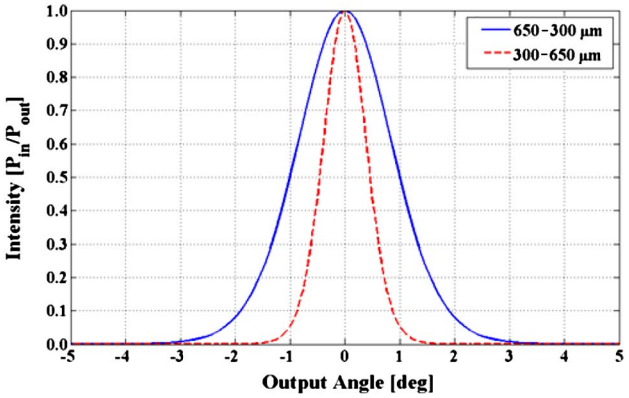

Fig. 2. Normalized power transmission as a function of output angle for increasing and decreasing bore tapered Ag/AgI HGW.

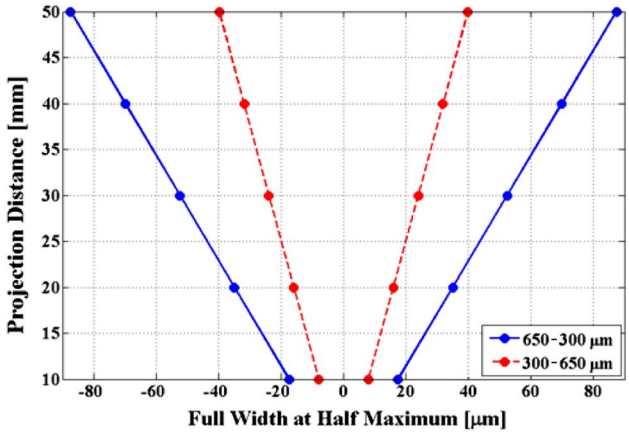

Fig. 3. Theoretical FWHM as a function of beam projection distance for determining divergence angles of tapered HGWs.

Through such qualitative and quantitative theoretical ray tracing analysis, current understanding of the effects of tapered HGW dimensionality on beam propagation may be advanced, allowing for the attainment of unconventional waveguiding behavior that may be difficult or impossible to achieve with constant bore size HGWs.

3. Fabrication Methodology

Tapered HGWs analyzed in this study were fabricated using conventional dynamic liquid deposition phase (DLPD) techniques for the deposition of high quality silver and subsequent silver iodide thin films in fused silica capillaries. Tapered fused silica capillaries serving as HGW substrates in this study were custom ordered from Polymicro, and were 200 cm in length with an approximately linearly varying inner diameter ranging from 300 to 650 μm along the capillary length. The experimental samples were first coated with a reflective silver (Ag) film approximately 1 μm in thickness and a subsequent dielectric silver iodide (AgI) thin film with thickness optimized for $\lambda = 9$–11 μm.

A. Dynamic Liquid Phase Deposition Methodology

The fabrication of Ag/AgI coated tapered HGWs is carried out via DLPD processes in which high quality thin films may be deposited with adequate control

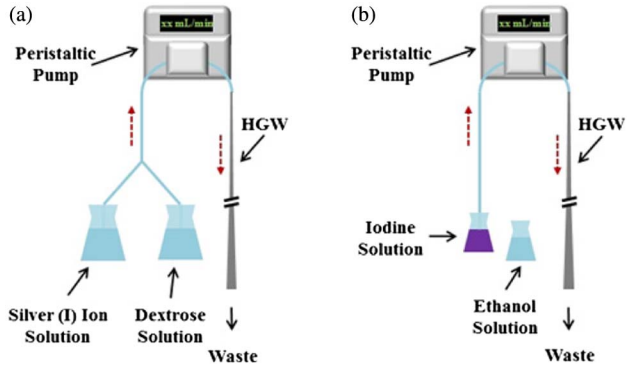

Fig. 4. (a) Silver film deposition and (b) iodization procedures.

from chemical precursor containing solutions. The DLPD process allows for the deposition of high quality thin films exhibiting high thickness uniformity both radially as well as along the entire sample length up to lengths of approximately 500 cm. The DLPD process involves the use of a peristaltic pump to flow precursor solutions at a predetermined fluid velocity through the fused silica capillary waveguide substrate for a desired amount of time. This allows for reaction of precursors in solution and subsequent thin film deposition of reactant species on the inner surface [1].

In determining optimal DLPD processing parameters, the sample dimensions must be taken into consideration, particularly as the reaction kinetics and deposited film quality are strongly affected by the peristaltic pump speed determined volumetric flow rate of solutions through the experimental sample. In practice, the volumetric flow rate must be optimized for the sample to be processed so as to maximize volumetric flow rate, thus increasing film quality and uniformity, while at the same time preventing excessive pressure buildup in the system, thus leading to irregular flow dynamics and undesirable effects. Fluid pressure buildup poses a pronounced challenge in small bore waveguides, and due to the largely length-dependent bore size profile of the tapered structures in this study, it proved to impose an additional challenge for the tapered HGWs in this study. In particular, the dynamic bore size of the tapered samples limited the overall possible volumetric flow rate of the system to rates commonly used for smaller bore waveguides, with a necessity to flow solutions in the direction of increasing bore size so as to prevent further fluid pressure increases that would occur in the case of fluid flow along the direction of decreasing bore size. Experimentally, the maximum flow rate achievable without the appearance of excessive pressure related effects was determined to be approximately 5.50 mL/min, corresponding to the optimal flow rate for fabrication of a 410 μm constant ID HGW. In contrast, the optimal flow rates for fabrication of 300, 475, and 650 μm ID HGWs are 3.0, 7.4, and 13.9 mL/min, respectively.

B. Deposition of Ag and AgI Films

Beginning with the fused silica capillary HGW substrates, fabrication of Ag/AgI HGWs consists of the deposition of a silver film and a subsequent dielectric silver iodide thin film. Prior to the silver film deposition procedure, the inner capillary surface is sensitized by pumping an acidic 1.55 mM stannous chloride solution at $T = 20°C$ for 5 minutes at the desired flow rate (5.50 mL/min in this case), allowing for simultaneous reduction of the necessary silver film deposition procedure time and the improved deposited silver film quality.

Upon completion of the sensitization procedure, deposition of the silver film is carried out. This is achieved by simultaneously pumping a 3.11 mM reducing dextrose solution and a caustic 14.36 mM ammonia-complexed silver (I) nitrate solution at equal rates through the waveguide bore using a peristaltic pump. Effectively, this allows for a 50:50 mixture of solutions flowing through the sample at the desired volumetric flow rate for the desired length of time, depositing a silver film on the sensitized inner fused silica surface. In practice, the film thickness must exceed that of the skin depth of silver plus that of the subsequent desired AgI film for optimal performance. For this study, the silver film deposition procedure was carried out for 30 minutes, yielding a film thickness of approximately 1 μm. The setup for the silver deposition procedure is depicted in Fig. 4(a).

Deposition of the dielectric AgI thin film is then performed by pumping a 39.40 mM elemental iodide solution in cyclohexane at $T = 15°C$ through the silver coated waveguide at the desired flow rate. This results in a subtractive reaction between the iodine solution and deposited silver film in which the silver film is converted to silver iodide. Given that this Ag to AgI mechanism rate is diffusion governed, the duration of iodization procedure time determines the radial amount of Ag converted to AgI and therefore the AgI film thickness. The iodization procedure used in this study is depicted in Fig. 4(b). In this study, the tapered HGWs were to be optimized for peak performance between $\lambda = 9$–11 μm, corresponding to AgI film thicknesses of $d_F = 0.77$–0.95 μm as determined by Eq. (5) [9]:

$$d_F = \frac{\lambda}{2\pi\sqrt{n_F{}^2 - 1}} \tan^{-1}\left(\frac{n_F}{\sqrt[4]{n_F{}^2 - 1}}\right), \tag{5}$$

where λ is the target wavelength in micrometer and n_F is the refractive index of the dielectric ($n_{\mathrm{AgI}} = 2.10$). To achieve an AgI film thickness within this desired range, the iodization procedure was carried out at a flow rate of 5.50 mL/min for 360 s [9].

4. Experimental Analysis

Characterization of experimental samples involved spectroscopic analysis at IR wavelengths, laser attenuation measurements, and beam profile analysis.

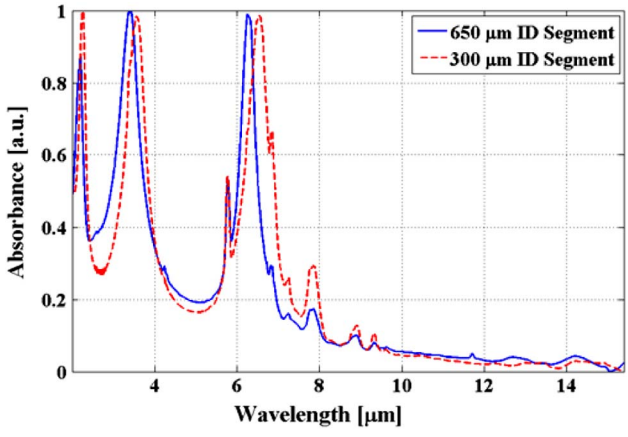

Fig. 5. IR spectral response of tapered Ag/AgI HGW sample.

FTIR spectroscopy was carried out to determine the optical response from $\lambda = 2$–15 μm using a Bruker Tensor 37 FTIR spectrometer in conjunction with a cryogenic MCT/A detector. Laser measurements were carried out at $\lambda = 10.6$ μm using a Synrad I-series 5 Watt maximum output CW CO2 laser with spatial power density distribution profiles obtained using a Spiricon am I 124 by 124 pixel pyroelectric beam profiler.

A. IR Spectral Response

The optical response of the experimental Ag/AgI coated tapered HGW samples in the near and mid-IR regime was obtained via FTIR spectroscopy. The first and last 14 cm of the fabricated samples were used as representative samples for determining the optical response of the tapered HGWs. By analyzing the initial and final segments of the waveguide sample, the optical response of the sample can be determined while simultaneously gaining insight as to the possible variability of AgI dielectric thin film along the waveguide length. Using this method, the IR spectral response of the Ag/AgI tapered HGWs was obtained and is shown in Fig. 5. From the first interference peak position seen in the IR spectral response of the Ag/AgI tapered HGW segments, the AgI dielectric thin film thickness can be calculated and was determined to be approximately $d = 0.850$–0.890 μm, which is within the desired range of $d = 0.773$–0.945 μm. From Fig. 5, we see some variability in AgI thin film optical response between the two samples, suggesting film thickness variation of approximately 0.040 μm along the 200 cm sample length. However, while the AgI film thickness is seen to increase slightly as a function of length, the optical response throughout the target wavelength range is consistent throughout the entire sample length. Therefore, it can be concluded that this small variation in dielectric film thickness has an insignificant impact on the functionality of the HGWs at the target wavelength range and can be practically regarded to be negligible. In addition to achieving a high degree of thin film uniformity, the narrow width of the interference peaks suggest that this fabrication methodology has proven successful in depositing high quality optical thin films in tapered HGWs for low-loss transmission at mid-IR wavelengths.

B. Attenuation Measurements

Attenuation measurements for the 200 cm long tapered HGW samples at $\lambda = 10.6$ μm were obtained for straight and several bent waveguide configurations. Using this methodology, the effects on the IR waveguiding properties of tapered HGWs under an applied curvature could be experimentally analyzed and compared to those of constant bore HGWs of comparable dimensions. The experimental setup for attenuation measurements involved coupling a 6.5 mm FWHM diameter CW CO_2 laser beam into the HGW sample with either a 76.2 or 127.0 mm focal length ZnSe length depending on whether the input ID for measurements was 300 or 650 μm, respectively. The first 50 cm of the waveguide samples were kept straight, while the next 140 cm of the sample were subjected to a predetermined constant curvature and the final 10 cm of the waveguide were kept straight. Output power measurements were then taken at applied bending radii of 10, 14, 18, 50, 75, 100, 150, 200, and 250 cm, as well as for a configuration in which the samples were kept straight. To determine the attenuation of the samples while minimizing experimental error due to coupling inefficiencies, the cutback method was utilized to calculate the loss where the input power was the power output measured out of the first 10 cm of the waveguide samples.

The attenuation as a function of curvature was obtained for the tapered Ag/AgI HGWs using both IDs as input as well as for 300 and 700 μm constant ID Ag/AgI HGWs of equal AgI film thickness to allow for accurate experimental comparison of results. The attenuation as a function of applied curvature for these 200 cm long experimental samples is given in Fig. 6. From Fig. 6, one can see that all waveguide samples follow the general $1/r$ bending loss dependence where the slope of the linear best fit denotes the sensitivity of the HGW attenuation to applied bending. As predicted by theoretical analysis, the straight losses for the tapered guides are lower than that of the 300 μm constant ID HGW but greater than that of the 700 μm constant ID HGW. Straight losses (curvature equal to 0) for all waveguide samples were considerably greater than those predicted by theory. These increased losses arise from a number of factors not accounted for in calculations including coupling inefficiencies, scattering losses arising from surface roughness, and increased attenuation due to lossy, higher order modes. Additionally, it can be seen that the loss for the tapered waveguides does depend on which bore size is used the input end, contradicting theoretical results. The experimental loss is in fact higher when a smaller ID size is used as the input. This discrepancy with theory may be logically attributed to coupling efficiency differences for the two

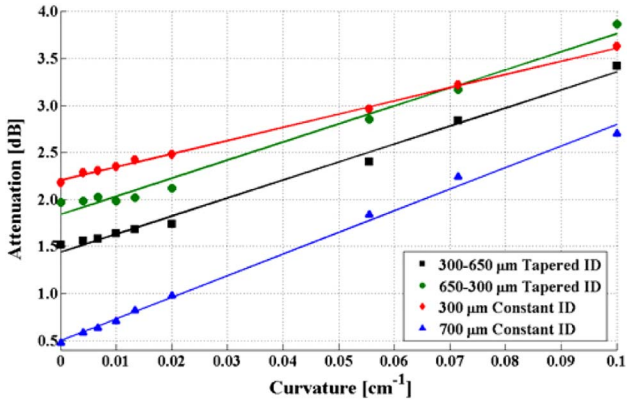

Fig. 6. Attenuation as a function of bending for tapered and constant bore HGWs with AgI film thickness $d \approx 880$–890 nm.

bore sizes, as higher order modes would experience considerably lower coupling efficiency when being launched into a 300 μm ID HGW than into a 650 μm ID HGW. Consequently, inherently lossier higher order modes, which would not be successfully coupled when using the 300 μm ID as input, would not contribute to the overall waveguide loss. This results in a lower overall measured loss than when these modes do contribute to the overall loss as in the case of using the 650 μm ID end as the input.

While the total loss of the tapered HGWs is dependent on what bore size is used as input, it should be noted that the bending loss dependence is in fact independent of which bore size is used as input, as seen by the near parallel nature of the best fit lines when using the 300 μm ID end as input and the 650 μm ID end as input. The corresponding slopes are determined to be 19.18 and 19.21 dB cm, respectively. Furthermore, the bending loss dependence of the tapered HGWs is larger than that for the 700 μm constant ID HGW at 23.02 dB · cm but less than that for the 300 μm constant ID HGW at 14.06 dB · cm. The increasing bending loss dependence with increasing bore size is due to the additional loss of higher order modes on bending in these highly over-moded waveguide structures where the bore size is much greater than the wavelength of propagating light [10]. As a larger number of higher order modes may be coupled into and propagate in larger HGWs, and as higher order modes are more susceptible to high bending losses, overall bending losses in larger HGWs increase faster than for smaller HGWs. From a ray optics perspective, this can be attributed to the higher losses experienced by propagating rays with larger initial propagation angles corresponding to higher order modes that can successfully couple into larger bore HGWs but not into smaller bore HGWs. As such, for any given HGW bore size, there is a trade-off between total straight power loss and additional bending power loss [10]. Tapered HGWs, however, pose an attractive partial solution to this fundamental trade-off, as lower overall losses than those achievable with smaller ID HGWs may be achieved while simultaneously allowing for a lower bending loss sensibility than that of larger bore HGWs.

C. Beam Profile Measurements

Analysis of the beam-propagating properties of the tapered HGW involved measuring the output spatial power density distribution using a Spiricon am I pyroelectric beam profiler at a fixed distance from the waveguide end. Initially, such analysis involved measuring the output beam profile at distances of 10, 20, 30, 40, and 50 mm from the waveguide end in the straight configuration to determine the divergence of the output beam. Figure 7 gives the 2D profiles of the spatial density distributions measured at selected distances from the HGW output that were used to experimentally obtain the divergence of the output beam using both the 300 μm ID end and the 650 μm ID end as input. The experimentally

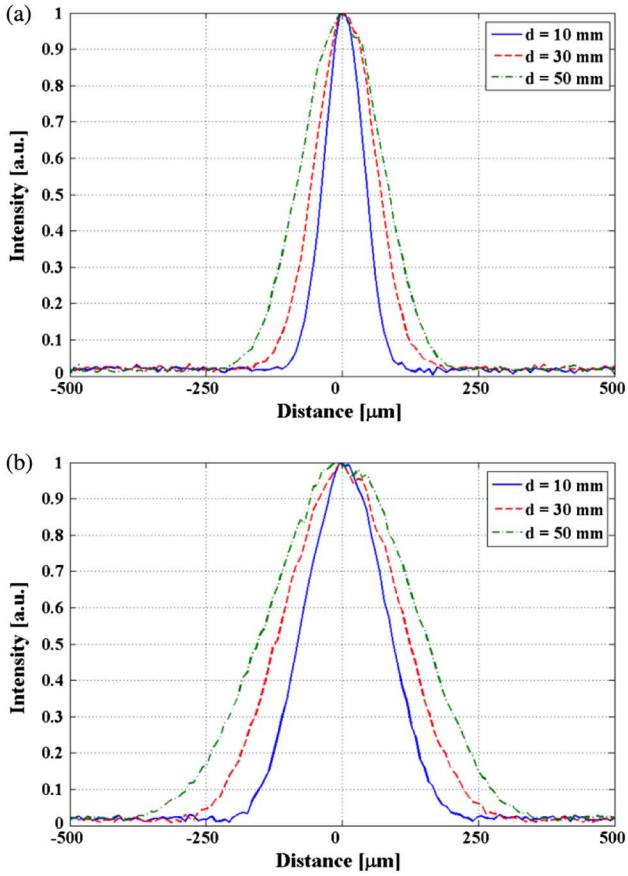

Fig. 7. 2D spatial power density distribution profile using the (a) 300 μm ID and (b) 650 μm ID end as input at $d = 10$, 30, and 50 mm.

calculated half-angle divergence values for the two cases were 0.116° and 0.199° using the 300 μm ID and 650 μm ID ends as input, respectively. As expected from the theoretical analysis, the spatial power density distribution is narrower when using the 300 μm ID end of the tapered HGW as input than when using the 650 μm ID end as input. Furthermore, the divergence is smaller in the former than in the latter case.

To determine the effects of bending on output beam propagation, the preceding method to determine beam divergence was repeated at bending radii of 50 and 10 cm. Table 3 gives the experimentally derived divergence values for the straight and bent waveguide samples using both the 300 μm ID end the 650 μm ID end as inputs. From the divergence measurements presented in Table 3, it can be seen that when using the 300 μm end as input, the output beam divergence decreases on increased bending, while conversely, it increases with increased bending

Table 3. Measured Output Beam Divergence

	300 μm Input	650 μm Input
$R = 0.0$ cm	0.116°	0.199°
$R = 50.0$ cm	0.102°	0.213°
$R = 10.0$ cm	0.090°	0.250°

when using the 650 μm ID end as input. This behavior, along with an increased loss on bending, may be attributed to an increased number of reflections experienced by a propagating beam when the waveguide is bent versus when it is kept straight. Thus, bending the guide results in increased loss and an increase in divergence when light propagates along the direction of decreasing bore size but in a decrease in divergence

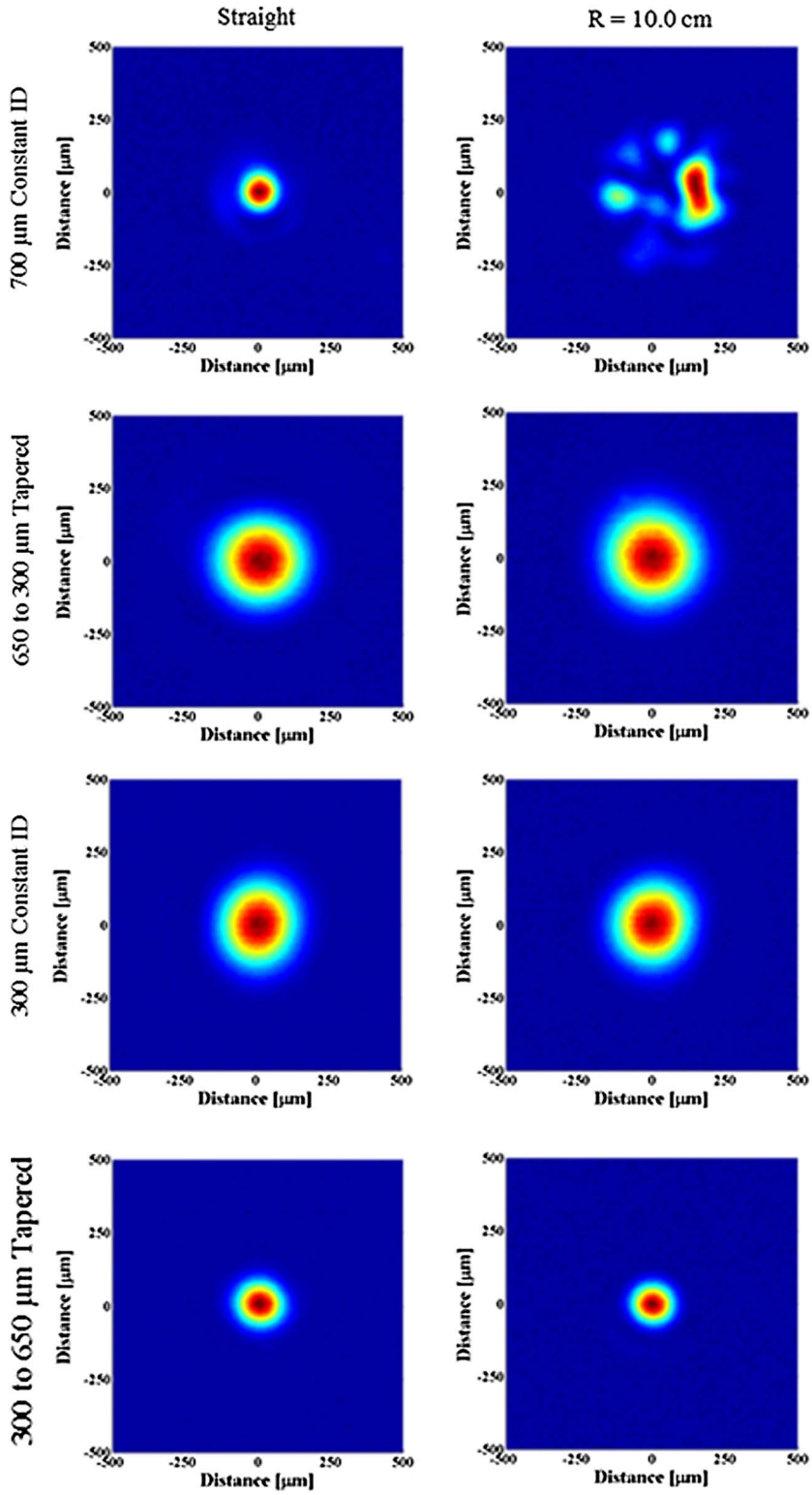

Fig. 8. Output beam profiles at $d = 30$ mm for straight and bent (a) 700 μm constant ID, (b) decreasing 650 – 300 μm tapered ID, (c) 300 μm constant ID, and (d) increasing 300–650 μm tapered ID Ag/AgI HGWs.

when light propagates along the direction of increasing bore size as predicted by Eq. (4).

Final analysis of the output spatial density distributions from tapered HGWs involved qualitative comparison of output beam profiles measured for tapered samples using both sides as input as well as comparable 300 and 700 μm constant ID HGWs. The profiles were measured at a distance of 30 mm from the waveguide output at straight (0) and 10 cm bending radii. Figure 8 gives the 2D contours for the straight and bent measured beam profiles for each sample. In comparing the output beam profiles (Fig. 8) obtained from both constant and tapered ID HGWS, several observations can be made. First, in contrasting the 300 and 700 μm constant ID HGWs, it can be seen that the beam quality is much better for the case of the smaller ID. This is because, while both HGW structure dimensions support multimode propagation, the attenuation of higher order modes increases as bore size decreases. The ability to couple a large number of modes into HGWs, each experiencing a different loss, furthermore allows for HGWs to be used as dimensional-dependent modal filters [10]. Furthermore, subjecting HGWs to external bending results in mode mixing and higher order mode generation, generally resulting in decreasing output beam quality with increased curvature. This is particularly dramatic for larger ID HGWs, as exemplified by the highly multimode output from the bent 700 μm ID HGW seen in Fig. 8(a). In comparing the tapered HGW with the 700 μm ID HGW, perhaps the most interesting difference is that a high output beam quality is seen in the case of the tapered HGW, even with considerable bending, thus supporting the experimentally and theoretically derived conclusions regarding unconventional beam propagation in tapered HGWs. While comparison of the tapered HGW beam profiles with the 300 μm ID HGW yields less dramatic differences, in-depth divergence analysis as performed for the tapered HGW profiles was likewise carried out for the 300 μm ID HGW. From such analysis, it was concluded that unlike for the tapered HGWs, beam divergence did not appreciably change for this constant ID HGW upon applied bending. This interesting result supports theoretical ray tracing analysis in constant bore HGWs that differs from tapered HGWs in that the angle of propagation is independent of the number of reflections and therefore remains constant despite an increased number of reflections resulting from increased bending. Furthermore, from Figs. 8(b) and 8(d) qualitative evidence of beam propagation properties previously derived quantitatively can be seen. When propagation occurs along the direction of decreasing bore size, an increase in both spot size and beam divergence is seen [Fig. 8(b)]. Alternatively, for propagation along the direction of increasing bore size, a decrease in both spot size and beam divergence upon increased bending is seen [Fig. 8(d)]. From the preceding analysis, it can be concluded that tapered HGWs are capable of achieving unconventional beam propagating properties relative to constant ID HGWs, including high quality beam propagation despite the large bore sizes, curvature-dependent spot size, and modification of output beam divergence through dimensional (taper gradient and/or waveguide length) alteration.

5. Conclusion

In this treatment, infrared beam propagation in silver/silver halide hollow waveguides of linearly length-varying (tapered) bore size is theoretically and experimentally investigated. Numerical analysis of beam propagation in constant bore and tapered bore HGWs based on ray tracing simulations shows that due to the length-varying ID size of tapered HGWs, the angle of propagation is dynamic and depends on the number of reflections (waveguide length), the taper gradient, and whether light propagates along the direction of increasing or decreasing bore size. This behavior is largely responsible for many of the atypical beam propagation properties of tapered HGWs including the reduction of loss sensitivity to bending, output beam narrowing and widening, and considerable change of beam divergence on bending. Subsequent experimental procedures were successful in fabricating low-loss IR transmissive Ag/AgI tapered HGWs, and experimental measurements supported the presented theoretical analysis. As a result of their unconventional light propagation properties, tapered HGWs present attractive alternatives to constant bore HGWs for applications requiring crucial precision of spot size and beam divergence. Additionally, tapered HGWs are capable of delivering a high-quality output beam comparable to that of smaller constant-bore HGWs while simultaneously achieving lower losses. On the other hand, tapered HGWs are capable of delivering much higher quality output beams than larger constant bore HGWs while simultaneously experiencing reduced bending losses albeit suffering from slightly higher overall transmission losses. Through the use of tapered HGWs, it is also possible to control the output beam properties *in situ*, most notably controlling the output spot size and beam divergence by applying a controlled bend and/or altering the waveguide length. Furthermore, by changing the tapered HGW dimensions, whether by changing the waveguide length, the taper gradient, and/or the range of ID sizes of the taper, the waveguide may be optimized to achieve a small output beam. In practice, the unconventional behavior of tapered HGWs make them attractive for use in a variety of applications, ranging from fast-tapered short HGWs for mode filtering, to slow-tapered long HGWs for laser delivery and remote sensing.

The authors would like to thank Dr. Jason M. Kriesel and Opto-Knowledge Systems (OKSI) of Torrence, California, USA, for their support in the success of this research initiative.

References

1. J. A. Harrington, *Infrared Fiber Optics and Their Applications* (SPIE, 2004).

2. M. Miyagi and S. Kawakami, "Design theory of dielectric-coated circular metallic waveguides for infrared transmission," IEEE J. Lightwave Technol. **LT-2**, 116–126 (1984).
3. D. J. Gibson and J. A. Harrington, "Tapered and noncircular hollow glass waveguides," Proc. SPIE **3596**, 8–13 (1999).
4. D. J. Gibson and J. A. Harrington, "Gradually tapered hollow glass waveguides for the transmission of CO_2 laser radiation," Appl. Opt. **43**, 2231–2235 (2004).
5. C. M. Bledt, D. V. Kopp, J. A. Harrington, S. Kino, Y. Matsuura, and J. M. Kriesel, "Investigation of tapered silver/silver halide coated hollow glass waveguides for the transmission of CO_2 laser radiation," Proc. SPIE **8218**, 821802 (2012).
6. M. Miyagi, "Waveguide-loss evaluation in circular hollow waveguides and its ray-optical treatment," IEEE J. Lightwave Technol. **LT-3**, 303–307 (1985).
7. Y. Matsuura, M. Saito, and M. Miyagi, "Loss characteristics of circular hollow waveguides for incoherent infrared light," J. Opt. Soc. Am. A **6**, 423–427 (1989).
8. E. D. Palik and G. Ghosh, *Handbook of Optical Constants of Solids* (Academic, 1998).
9. K. Matsuura, Y. Matsuura, and J. A. Harrington, "Evaluation of gold, silver, and dielectric-coated hollow glass waveguides," Opt. Eng. **35**, 3418–3421 (1996).
10. C. M. Bledt, J. A. Harrington, and J. M. Kriesel, "Loss and modal properties of Ag/AgI hollow glass waveguides," Appl. Opt. **51**, 3114–3119 (2012).